J Mater Sci: Mater Electron (2014) 25:4163–4169
DOI 10.1007/s10854-014-2144-3

Annealing temperature dependence on the structural and optical properties of sputtering-grown high-k HfO_2 gate dielectrics

B. Deng · G. He · X. S. Chen · X. F. Chen · J. W. Zhang · M. Liu · J. G. Lv · Z. Q. Sun

Received: 19 April 2014 / Accepted: 1 July 2014 / Published online: 9 July 2014
© Springer Science+Business Media New York 2014

Abstract High-k gate dielectric HfO_2 thin films have been deposited on Si and quartz substrates by radio frequency magnetron sputtering. The structural characteristics, surface morphology, and optical properties of the HfO_2/Si gate stacks at various post-annealing temperatures were examined by X-ray diffraction (XRD), atomic force microscopy (AFM), fourier transform infrared spectroscopy (FTIR), ultraviolet–visible spectroscopy (UV–Vis spectroscopy), and spectroscopic ellipsometry (SE). XRD measurement indicates that the 80 W-deposited HfO_2 films demonstrate a polycrystalline structure. AFM measurements illustrate that the root mean square of the HfO_2 thin films demonstrates an apparent increase with increasing the annealing temperature. Analysis from FTIR indicates that the Si–O–Si bonds vibration peak position shift toward lower wave numbers with increasing the annealing temperature. Combined with UV–Vis spectroscopy and SE measurements, it can be noted reduction in band gap with an increase in annealing temperature has been confirmed. Additionally, increase in refractive index (*n*) has been confirmed by SE.

B. Deng · G. He (✉) · X. F. Chen · J. W. Zhang · Z. Q. Sun
School of Physics and Materials Science, Anhui University, Hefei 230601, People's Republic of China
e-mail: ganghe01@issp.ac.cn

G. He · X. S. Chen
National Laboratory for Infrared Physics, Chinese Academy of Sciences, Shanghai Institute of Technical Physics, 500 Yutian Road, Shanghai 200083, People's Republic of China

M. Liu
Key Laboratory of Materials Physics, Anhui Key Laboratory of Nanomaterials and Nanostructure, Institute of Solid State Physics, Chinese Academy of Sciences, Hefei 230031, People's Republic of China

J. G. Lv
Department of Physics and Electronic Engineering, Hefei Normal University, Hefei 230061, People's Republic of China

1 Introduction

Over the last few decades silicon dioxides have been used successfully in gate dielectrics application. However, with the quick development of microelectronics, the size of complementary metal-oxide-semiconductor filed effect transistor (CMOSFET) is becoming smaller and smaller on the basis of the "Moore law", the thickness of SiO_2 gate dielectric is approaching its physical limits. So the investigation of high-k gate dielectric materials for next generation MOSFET applications has been paid more attention [1–3].The suitable high-k gate dielectrics should have reasonably high dielectric constant, a relatively large band gap, high heat of formation, and good thermal stability on Si against reactions with the formation of SiO_2 interface [4]. Materials such as $SrTiO_3$, Ta_2O_3, Al_2O_3, TiO_2, ZrO_2, and HfO_2 have been investigated extensively for such applications [5–12]. Among these high-k gate dielectrics, HfO_2 is the most promising alternative materials due to its high dielectric constant, large band gap and thermal stability in contact with silicon.

The fabrication technology of Hf-based high-k ultrathin gate dielectrics can be categorized into three major approaches based on the reaction mechanism during preparation, namely solution deposition, chemical vapor deposition (CVD) [13, 14], and physical vapor deposition (PVD) processes [15, 16]. Solution-based methods mainly include sol–gel, metal–organic decomposition, and so on [17–19]. Compared to the solution deposition and chemical vapor deposition, the advantages of PVD-based deposition method

included easily controllable growth of the low-k interfacial layer at low temperature and compositional consistency between the target and the deposited film [20–22]. However, the RF sputtering is one of the most feasible methods in fabricating high-quality thin films with inherent versatility and the capability of obtaining a homogeneous surface coverage at low temperatures under controlled processing conditions. Above all, oxide films' size, shape and distribution deposited by RF sputtering can be controlled by a proper choice of preparation parameters like RF-power, operating pressure, plasma atmosphere, substrate temperature and deposition time. Based on mentioned advantages, in current paper, we pay attention to present some recent progresses of Hf-based gate dielectrics grown by PVD-based techniques. By far, although there exist some work related to HfO_2 high-k gate dielectrics, much of them have been focused on the investigation of the interfacial and electrical properties of HfO_2-based MOS. As we know, the change of HfO_2 thin films on the structure after post-deposition annealing is very large. However, the surface structure of the material is also one of the most factors affecting the optical properties of the material [23]. So, the investigation of the effects of post-deposition annealing on structure and optical properties is very necessary. Additionally, combined with ultraviolet–visible spectroscopy (UV–Vis spectroscopy) and spectroscopy ellipsometry (SE) measurements, the optical band gap of sputtering-derived HfO_2 thin films have been studied correctly.

2 Experimental details

Si substrates with resistivity of 2–5 Ω/cm were cleaned by a modified RCA method, then the substrates were immersed in HF (1 %) solution for 30 s to remove any native oxide and rinsed with ionized water. After dying the wafers with pure N_2 gas, the Si substrates were put into vacuum chamber quickly. High purity HfO_2 ceramic target (99.995 %) with diameter of 60 mm and thickness of 5 mm was used as the sputtering target. High purity Ar (99.999 %) was introduced into the chamber during deposition. The substrate-target distance was maintained at 60 mm. The deposition temperature was room temperature. Prior to HfO_2 thin film deposition, the target was pre-sputtered in an argon atmosphere for 5 min to remove the surface oxide of the target. The Ar flow rate was kept at 20 SCCM and the base vacuum was higher than 1.0×10^{-4} Pa. The RF power and the working pressure were fixed at 80 W and 0.35 Pa during the sputtering process. The deposition time was 1.5 h. To investigate the effect of the high temperature annealing on the thermal stability of HfO_2/Si system, post-deposition annealing was conducted under oxygen ambient with temperature of 400, 600 and 800 °C for 30 min, respectively. To explore the structure and optical properties preferably, the quartz plates were also chosen as the substrates. The transmittance of the quartz substrate is about 90 % in the wave band of 190–900 nm. Several characterization techniques were used for the physical analysis of the HfO_2 thin films. X-ray diffraction (XRD) has been used to characterize the microstructure, grain size, crystallization and phase transition of HfO_2 thin films related to annealing temperature. Analysis of the interfacial structure of HfO_2/Si as a function of post-deposition annealing temperature is also carried out by fourier transform infrared spectroscopy (FTIR). The atomic force microscopy (AFM) reveals the effect of post-deposition annealing on surface morphology of HfO_2 thin film. The ultraviolet visible spectroscopy (UV–Vis spectroscopy) and spectroscopy ellipsometry (SE) have been carried out to investigate the annealing temperature dependent optical constants of HfO_2 film.

3 Results and discussion

Post-deposition annealing temperature dependent structural properties of the as-deposited HfO_2 films were analyzed by XRD. Figure 1 shows the XRD patterns of HfO_2 films grown on the quartz substrate. The XRD measurements demonstrate that the HfO_2 films deposited at 80 W are polycrystalline structure. The dominant peak of the 80 W-derived HfO_2 film is at about 28.3°. It is attributed to the diffraction peak of (−111) planes of HfO_2 with monoclinic structure. After post deposition annealing, there are three dominant peaks appearing at 28.3°, 31.6° and 34.3°, which originates from the diffraction peak of (−111), (111) and (020) planes of HfO_2, respectively. Some weak peaks come from the orientation (−211), (112) and (220) of HfO_2 films [24]. According to the powder diffraction ICDD card (06-0.318), all the peak positions of HfO_2 films correspond to the monoclinic crystal structure and no diffraction peaks from cubic or tetragonal phase have been observed. Based on XRD patterns shown in Fig. 1, it can be noted that the intensity of the dominant peak (−111) of monoclinic HfO_2 increases with increasing the annealing temperature. These results clearly indicate that the film structure is dependent on the annealing temperature which plays an important role during the crystallization process. In order to attain the detailed structure information, the crystallite size of HfO_2 films has been calculated by using the (−111) crystal plane of HfO_2 films. Scherrer Equation has been adapted to work out the grain sizes as the following forms:

$$D_{hkl} = k\lambda/\beta\cos\theta \quad (1)$$

where D_{hkl} is grain sizes, $k = 0.89$, $\lambda = 0.1540$ nm; β is full width at half maximum; θ is diffraction angle. All the

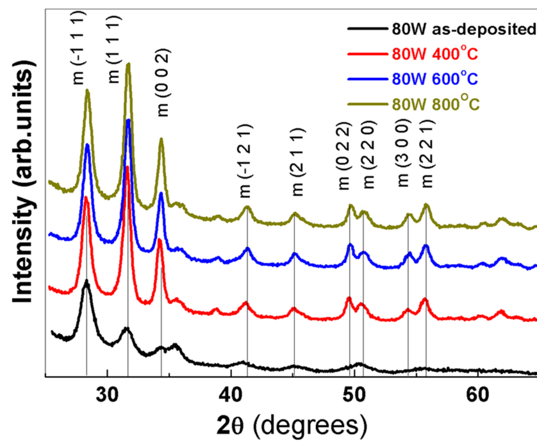

Fig. 1 XRD spectra of HfO_2 thin films annealed at various temperature

Table 1 The parameter of HfO_2 thin films by RF magnetron sputtering

	Grain sizes (nm)	RMS (nm)	Banf gap (eV)	Average transmission (%)
As-deposited	9.43	2.10	5.52	79.6
400 °C	11.6	2.26	5.50	73.9
600 °C	12.1	2.47	5.48	72.3
800 °C	12.2	2.85	5.41	71.5

calculated parameters has been shown in Table 1, Based on Table 1, it can be noted the crystallite size increases slightly as the annealing temperature increases from room temperature to 800 °C.

The effect of the post deposition annealing temperature on the surface morphology of the HfO_2 thin films has been investigated by AFM. Figure 2 shows the surface morphologies of the as-deposited and annealed HfO_2 samples at 400, 600 and 800 °C, which are scanned over areas of 2 μm × 2 μm. Based Fig. 2, it can be seen that the root mean square (RMS) roughness of the HfO_2 thin films increases with increasing the annealing temperature. According to our previous results, it is found that the film takes on a smoother surface below the crystallization temperature, resulting from the smaller grain size and lower surface atomic diffusion [25]. When annealed at high temperature, film surface again becomes rough, which is believed to be as a result of the crystallization-induced large grain size. Therefore, it can be concluded that post deposition annealing has obvious effect on the evolution of the morphology of Hf-based high-k gate dielectrics materials.

In order to ensure that Si–O bonding is associated with the interfacial layer, the infrared absorption spectra were obtained with the backside of all wafers etched in diluted HF solution to remove any native oxide and subtract the absorbance of the sample and a reference from the same wafer with no HfO_2 present. As a result, we detected signals from the interfacial SiO_2 films. Figure 3 shows the FTIR absorption spectra for the as-deposited and HfO_2 sample annealed at 400, 600, and 800 °C. From Fig. 3a, it can be see that the two peaks located at 505 and 605 cm^{-1} are assigned to the monoclinic phase of HfO_2 [26], which is in good agreement with previous XRD results presented in Fig. 1. To investigate the shift of peak position and the change of Si–O bond absorption intensity, infrared absorption spectra from 1,000 to 1,150 cm^{-1} have been selected, shown in Fig. 3b. The intensity of the absorption band increases after the post deposition annealing, indicating that the formation of the interfacial Si-oxide layer associates with the annealing temperature. What's more, the peak of Si–O stretching mode demonstrates an apparent red shift with the increase in annealing temperature, implying the possibility of formation of silicates [27].

The optical properties of the HfO_2 thin films deposited by RF sputtering were analyzed by UV–Vis spectroscopy. The transmission spectra of HfO_2 thin films sputtered on quartz substrate were investigated by spectrophotometer methods in the wavelength range of 190–900 nm at room temperature, as shown in Fig. 4. In order to figure out the average transmission, the wavelength from 300 to 900 nm has been selected. The average transmission is in the range of 70–80 % for all the studied samples. Based on Fig. 4, it can be noted that the average transmission of HfO_2 thin films decreases with the increase of the annealing temperature, which can be attributed to the increase of surface roughness and decrease the grain interface defect after post deposition annealing [28], which is in good agreement with the observation from AFM.

Figure 5 shows UV–Vis absorption spectra of the HfO_2 thin films annealed at different temperature. The energy band gap (E_g) value of the HfO_2 were obtained by absorption spectra and plotting $(\alpha h\nu)^2$ versus photon energy ($h\nu$) using the following relation:

$$(\alpha h\nu)^2 = A\left(h\nu - E_g\right) \tag{2}$$

where α is the absorption coefficient, A is the constant, and E_g is band gap, respectively. A plot of $(\alpha h\nu)^2$ vs ($h\nu$) is shown in Fig. 5 and the linear portion of the curve is extrapolated to $h\nu$ axis to determine the energy band gap. The measured optical band gap E_g values are given in Fig. 5. It can be seen that the band gap E_g decreases from 5.52 to 5.41 eV as the annealing temperature increases from room temperature to 800 °C, suggesting that red shift in optical band gap has been observed after post deposition annealing. According to previous reports [29–31], band gap

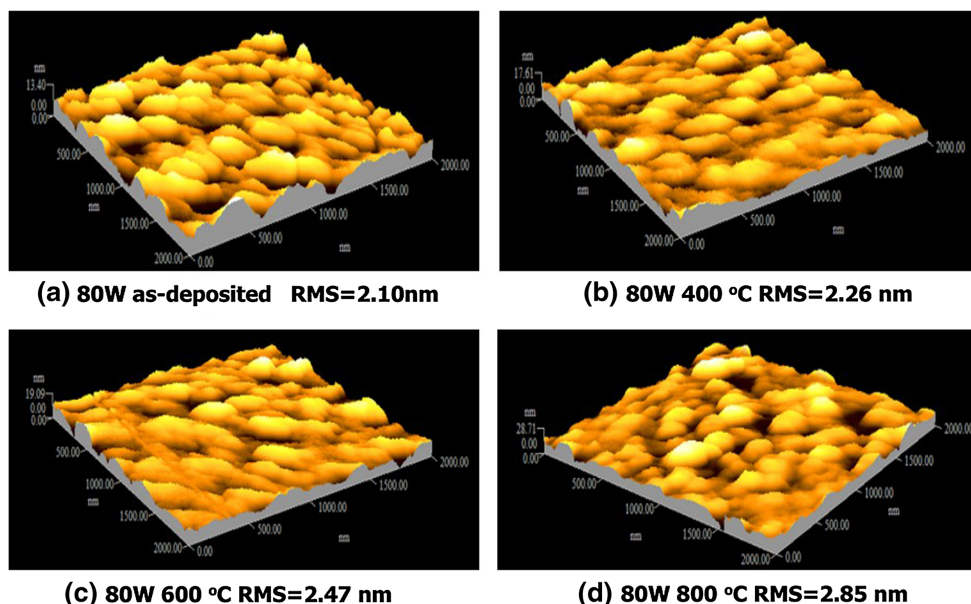

Fig. 2 AFM images of the as-deposited and annealed HfO_2 films: **a** as-deposited; **b** 400 °C, **c** 600 °C, and **d** 800 °C

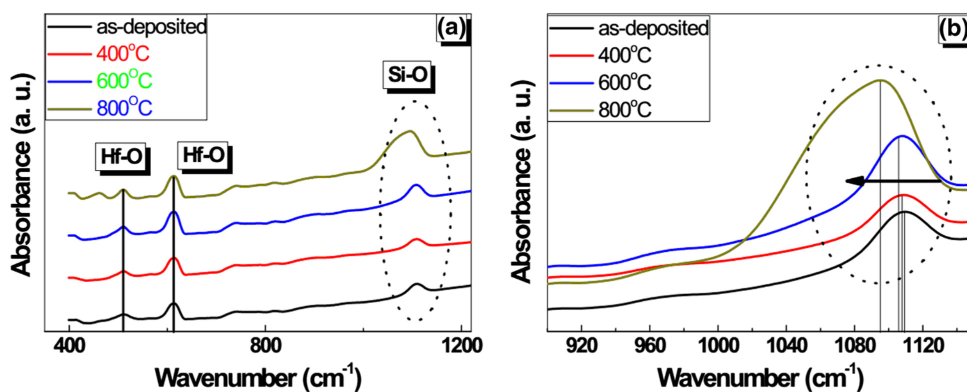

Fig. 3 FTIR spectra for the HfO_2 thin films annealed at various temperature

energies of 5.41–5.60 eV have been determined for crystalline HfO_2 films with monoclinic phase, which is close to our observation confirmed by XRD and FTIR. The optical band gap is affected by many factors such as defects density, purities, packing density, stoichiometric ratio and grain size [32, 33]. Liu et al. [34] proposed that the defects and disorders in the films will produce localized states in the band structure and thus result a low band gap value. But this statement is usually applied to amorphous materials but HfO_2 films are crystalline and not amorphous. In this paper, it is noted that the decrease of optical band gap attributed to the increase of the HfO_2 grain size after post-deposition annealing, agreed with the results of Hong et al. [35].In order to investigate further the annealing temperature dependent optical constant evolution, an ex situ SE (SC630) was applied to measure post deposition annealing temperature dependent optical functions of HfO_2 thin films at room temperature in the spectral range 190–1,100 nm.

The experimental parameters obtained by SE are the angles Ψ (azimuth) and Δ (phase change), which are related to the microstructure and optical properties, defined by:

$$\rho = r_p/r_s = \tan\psi \exp(i\Delta) \quad (3)$$

where r_p and r_s are the amplitude reflection coefficient for light polarized in the p- and s-planes of incidence, respectively. The spectral dependencies of ellipsometric parameters Ψ (azimuth) and Δ (phase change) can be fitted with appropriate models for the layer stacking structures and some appropriate optical constant or dispersion model for each layer. When appropriate modeling approaches have been developed, the optical properties of the film, such as refractive index n, extinction coefficient k, real part (ε_1) and imaginary part (ε_2) can be simultaneously extracted from ellipsometric parameters Ψ and Δ. The optical band gap also can be obtained by extinction coefficient k. In this paper, the Cauchy model was selected to

describe the unknown dielectric function of HfO_2, expressing in the following:

$$n(\lambda) = A_n + B_n/\lambda^2 + C_n/\lambda^4 \quad (4)$$

$$k(\lambda) = \alpha e^{\beta\left(1240/\lambda - E_g\right)} \quad (5)$$

Above equations as functions of the wavelength λ are uniquely defined by six parameters, A_n, B_n, C_n (index parameters which specify the index of refraction), α, β, and E_g, (absorption parameters that specify the shape of the absorption tail). In current work, a three layer model (HfO_2 film/SiO_2/Si) has been established to work out the optical function of the HfO_2 films related to post deposition annealing temperature. The measured and fitted spectra of a representative HfO_2 film at the incident angle of 65° and 75° are shown in Fig. 6. It can be clearly seen that an excellent agreement between the experimental and fitted spectra for the HfO_2 films has been attained in the entirely measured energy range, suggesting that the structured model is reasonable and can describe the structure of the as-deposited sample.

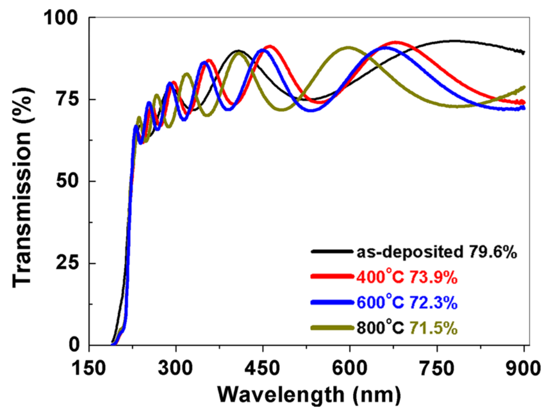

Fig. 4 Transmittance spectra of HfO_2 thin films annealed at different temperature

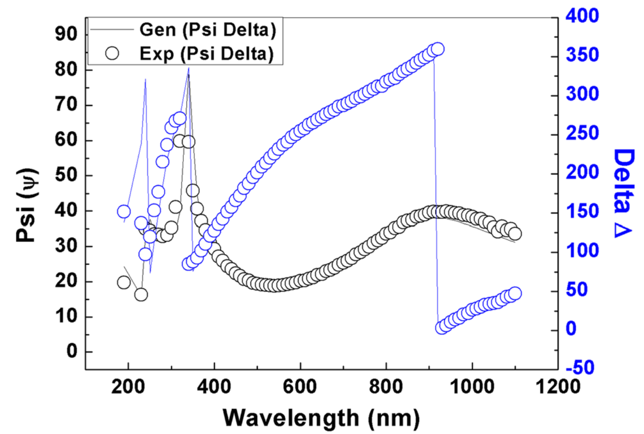

Fig. 6 The experimental and fitted spectroscopic ellipsometric data for the as-deposited HfO_2 film with deposition power of 80 W

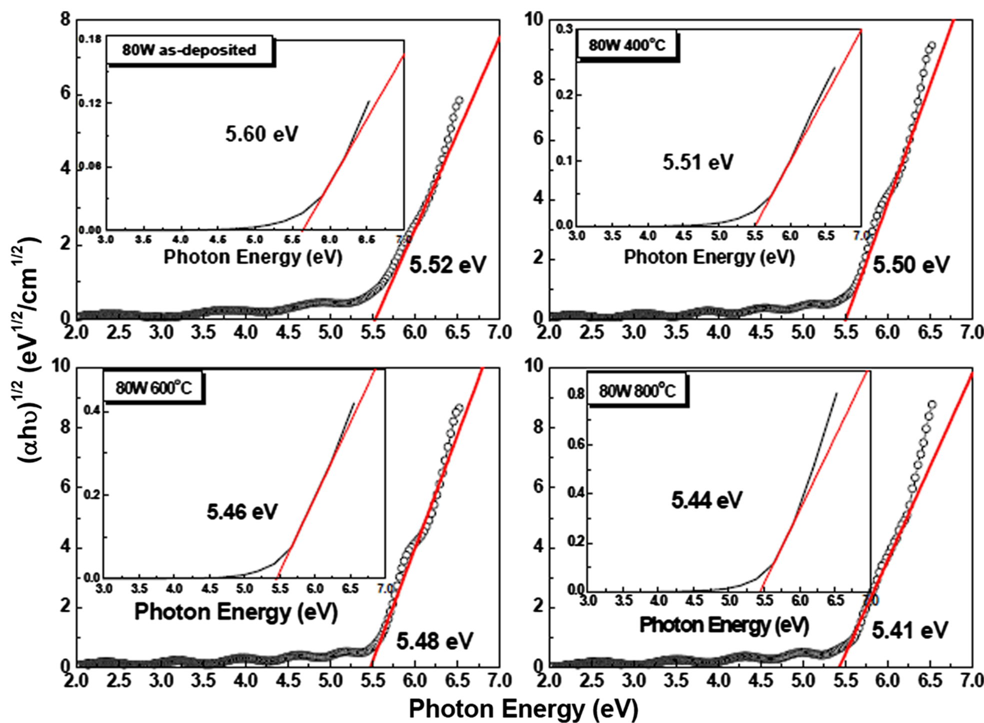

Fig. 5 UV–Vis absorption spectra of the HfO_2 thin films. *Insets* in Fig. 5 show the SE-derived plots of the $(\alpha h\nu)^{1/2}$ versus hν curve for the as-deposited and annealed HfO_2 films

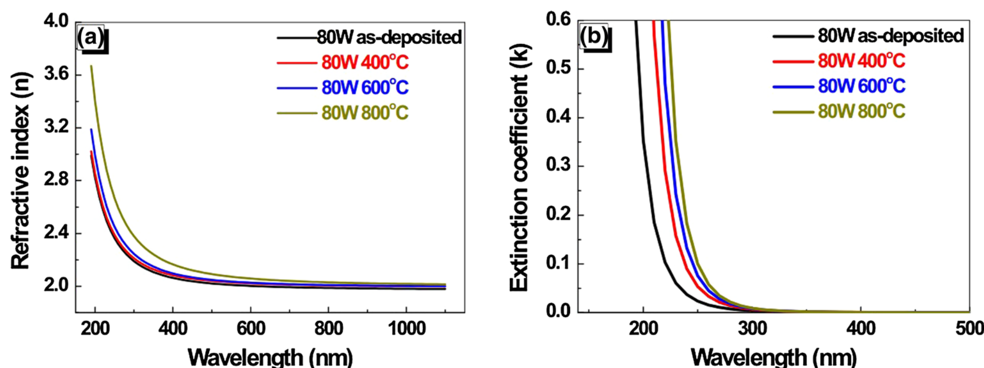

Fig. 7 The calculated refractive index and extinction coefficient dispersion relation of the HfO_2 films, derived from the results of the Cauchy fitting

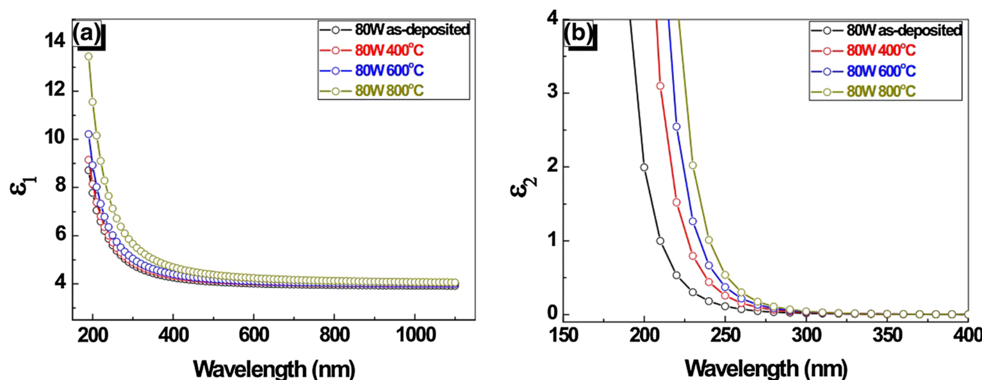

Fig. 8 The real (ε_1) and imaginary (ε_2) parts of the dielectric functions of HfO_2 films with various annealing temperature

Figure 7 shows the variation of the refractive index n and the extinction coefficient k for the as-deposited and annealed HfO_2 thin films. Shown in Fig. 7a, there is obvious increase in the value of refractive index with increasing the annealing temperature. It is noted that there are large and discontinuous increases in values of refractive index, which can be correlated with the increase of packing density. The refractive index of the as-deposited thin films is lower than that annealed thin films, which can be due to the loose arrangement. A higher refractive index is attributed to the formation of more closely packed thin films after high temperature annealing. Figure 7b shows the extinction coefficient spectra. It is noted that there is a slight red shift in the k tail edge after high temperature annealing, indicating the change in the optical absorption properties, agreeing with the results of UV–Vis spectroscopy. In addition, it can be seen that the extinction coefficient of the films is very low and close to zero, showing a very small optical loss because of absorption in the visible region.

The real (ε_1) and imaginary (ε_2) parts of the dielectric functions of HfO_2 with various annealing temperature are presented in Fig. 8. The real part of the dielectric function ε_1 ($\varepsilon_1 = n^2 - k^2$) is similar to n^2 and is related to polarization. The direct absorption edge is obtained from the imaginary part of the dielectric function $\varepsilon_2 = 2nk$. It noted that the HfO_2 thin films annealed at high temperature have higher ε_1 and ε_2 values compared to the as-deposited one, showing annealing temperature has magnificent effect on the dielectric properties. As we know, the dielectric function of HfO_2 thin film is strongly related to its microstructure and energy-band structure. There is an increase in the amplitude of the critical points within both real and imaginary part of dielectric function for that a transition from a disordered to a more ordered crystalline phase takes place in HfO_2 thin film, agreeing with the XRD results. To estimate the optical band gap values of the as-deposited and annealed HfO_2 thin films, SE data have been analyzed. The absorption coefficient α can be calculated by the following expression:

$$\alpha = 4\pi k/\lambda \tag{6}$$

where α is the absorption coefficient, λ is the light wavelength, and k is the extinction coefficient. So, the optical band gap can be extracted by extrapolating $[\alpha(E)E]^{1/2}$ to zero. The linear fit of the data indicates the characteristic

feature of the HfO_2 with an indirect band gap. Based on the insets in Fig. 5, band gap energies of 5.60, 5.51, 5.46, and 5.44 eV, for the as-deposited and annealed samples at 400, 600, and 800 °C, have been observed, respectively. The values of the band gaps for the HfO_2 thin films are very close to the results obtained by UV–Vis. Meanwhile, red shift in band gap related with annealing temperature is also observed, which agrees with the conclusion confirmed by UV–Vis spectroscopy.

4 Conclusions

In summary, the effects of post deposition annealing temperature on the structure and optical properties of HfO_2 thin films have been investigated by XRD, FTIR, AFM, UV–Vis spectroscopy, and SE. XRD analysis shows that the as-deposited HfO_2 films aren't amorphous but are in monoclinic phase. The crystallite size increases slightly as the annealing temperature from room temperature to 800 °C. AFM analysis shows the root mean square (RMS) roughness of the HfO_2 thin films increases with increasing the annealing temperature. FTIR analysis indicates the formation of the interfacial Si-oxide layer associates with the annealing temperature and there is an apparent red shift from 1,110 to 1,095 cm^{-1} along with the increased annealing temperature, indicating the formation of silicate layer. The optical properties related to post deposition annealing temperature have been investigated by UV–Vis spectroscopy and SE measurement. The increase in the refractive index and reduction in optical band gap have been observed as a function of annealing temperature.

Acknowledgments The authors acknowledge the support from Anhui Provincial Natural Science Foundation (1208085MF99), National Key Project of Fundamental Research (2013CB632705), Provincial Natural Science Foundation of Anhui Higher Education Institution of China (KJ2012A023), Key Project of Chinese Ministry of Education (212082), and Outstanding Young Scientific Foundation of Anhui University (KJJQ1103) and "211 project" of Anhui University.

References

1. G. He, L.D. Zhang, M. Liu, Appl. Phys. Lett. **95**, 112905 (2009)
2. G. He, G.W. Meng, L.D. Zhang, M. Liu, Appl. Phys. Lett. **91**, 232910 (2007)
3. G. He, B. Deng, H.S. Chen, X.S. Chen, J.G. Lv, Y.Q. Ma, Z.Q. Sun, APL. Mater. **1**, 012104 (2013)
4. G. He, Q. Fang, G.H. Li, J.P. Zhang, L.D. Zhang, Appl. Surf. Sci. **253**, 8483 (2007)
5. H. Yu, J.J. Wang, S.C. Yan, T. Yu, Z.G. Zou, J. Photoch. Photobiol. A **275**, 65 (2014)
6. M.K. Kim, W.H. Kim, Lee, H. Kim, Thin Solid Films **542**, 71 (2013)
7. L.Q. Zhu, Y.H. Liu, H.L. Zhang, H. Xiao, L.Q. Guo, Appl. Surf. Sci. **288**, 430 (2014)
8. L.F. Werner, R. Faccio, A. Juan, H. Pardo, B. Montenegro, A.W. Mombru, Appl. Surf. Sci. **290**, 180 (2014)
9. M. Taguchi, T. Nakane, A. Matsushita, Y. Sakka, T. Uchikoshi, T. Funazukuri, T. Naka, J. Supercrit. Fluid. **85**, 57 (2014)
10. G. He, L.D. Zhang, G.H. Li, M. Liu, L.Q. Zhu, S.S. Pan, Appl. Phys. Lett. **86**, 232901 (2005)
11. R. Jiang, E.Q. Xie, Z.F. Wang, J. Mat. Sci. **42**, 7343 (2007)
12. L.P. Feng, N. Li, H. Tian, Z.T. Liu, J. Mat. Sci. **49**, 1875 (2014)
13. E. Levrau, K. Devloo-Casier, J. Dendooven, K.F. Ludwig, P. Verdonck, J. Meersschaut, M.R. Baklanov, C. Detavernier, Langmuir **29**, 12284 (2013)
14. P. Verdonck, A. Delabie, J. Swerts, L. Farrell, M.R. Baklanov, H. Tielens, E. Van Besien, T. Witters, L. Nyns, S. Van Elshocht, Microelectron. Eng. **106**, 81 (2013)
15. G. He, B. Deng, Z.Q. Sun, X.S. Chen, Y.M. Liu, L.D. Zhang, Crit. Rev. Solid State Mater. Sci. **38**, 235 (2013)
16. S. Godavarthi, Q.T. Le, P. Verdoncka, S. Mardani, K. Vanstreels, E. Van Besien, M.R. Baklanov, Microelectron. Eng. **107**, 134 (2013)
17. M.S. Kim, Y.D. Ko, M. Yun, J.H. Hong, M.C. Jeong, J.M. Myoung, I. Yun, Mater. Sci. Eng. B **123**, 20 (2005)
18. J. Varghese, T. Joseph, M.T. Sebastian, AIP Conf. Proc. **1372**, 193 (2010)
19. T. Kawahara, M. Yamamuka, T. Makita, J. Naka, A. Yuuki, N. Mikami, K. Ono, Jpn. J. Appl. Phys. **33**, 5129 (1994)
20. J. Zuo, G.G. Nie, X. Gu, Y. Zong, L. Sun, C.J. Lin, Mater. Lett. **61**, 2632 (2007)
21. V. Kapaklis, P. Poulopoulous, V. Karoutsos, T. Manouras, C. Politis, Thin Solid Films **510**, 138 (2006)
22. J. Zuo, Appl. Surf. Sci. **256**, 7096 (2010)
23. Y.C. Liu, S.K. Tung, J.H. Hsieh, J. Cryst. Growth **287**, 105 (2006)
24. M.F. Al-Kuhaili, S.M.A. Durrani, I.A. Bakhtiari, M.A. Dastageer, M.B. Mekki, Mater. Chem. Phys. **126**, 515 (2011)
25. G. He, L.D. Zhang, J. Mater. Sci. Technol. **23**, 433 (2007)
26. M. Modreanu, J. Sancho-Parramon, O. Durand, B. Servet, M. Stchakovsky, C. Eypert, C. Naudin, A. Knowles, F. Bridou, M.F. Ravet, Appl. Sur. Sci. **253**, 328 (2006)
27. G. He, Q. Fang, M. Liu, L.Q. Zhu, L.D. Zhang, J. Cryst. Growth **268**, 155 (2004)
28. J. Aarik, H. Mandar, M. Kirm, Thin Solid Films **466**, 41 (2004)
29. A. Ramadoss, S.J. Kim, J. Alloys. Compd **544**, 115 (2012)
30. H. Kato, T. Nango, T. Miyagawa, T. Katagiri, K.S. Seol, Y. Ohki, J. Appl. Phys. **92**, 1106 (2002)
31. C.Y. Ma, W.J. Wang, J. Wang, C.Y. Miao, S.L. Li, Q.Y. Zhang, Thin Solid Films **545**, 279 (2013)
32. S. Prucnal, J.M. Sun, A. Nazarov, L.P. Tjagulskii, L.N. Osiyuk, R. Fedaruk, W. Skorupa, Appl. Phys. B. **88**, 241 (2007)
33. X. Liu, D. Li, Appl. Surf. Sci. **253**, 2143 (2006)
34. M. Liu, Q. Fang, G. He, L. Li, L.Q. Zhu, G.H. Li, L.D. Zhang, Appl. Phys. Lett. **88**, 192904 (2006)
35. R. Hong, J. Huang, H. He, Z. Fan, J. Shao, Appl. Surf. Sci. **242**, 346 (2005)